

ORIGINAL ARTICLE**Full-field measurement of contact-point and crack-tip deformations in soda-lime glass. Part-II: Stress wave loading****Balamurugan M. Sundaram**  | **Hareesh V. Tippur** Department of Mechanical Engineering,
Auburn University, Auburn, AL**Correspondence**

Hareesh V. Tippur

Email: tippuhv@auburn.edu

Funding information

Army Research Office, Grant/Award

Number: W911NF-16-1-0093, W911NF-15-1-0357 (DURIP)

Abstract

Transparent brittle ceramics such as soda-lime glass pose unique challenges for performing full-field optical measurement of deformations and stresses to characterize fracture and failure behaviors. Low fracture toughness coupled with high stiffness and elastic wave speeds are among the factors responsible for some of these challenges as deformations tend to be confined to an extremely small region near an almost mathematically sharp growing crack. Need for strong birefringence, elaborate optics, or lack of sufficient measurement sensitivity are some of the factors against legacy techniques such as photoelasticity, optical interferometry, and speckle methods, respectively, to study soda-lime glass. Motivated by these factors, the feasibility of digital gradient sensing (DGS) method to measure impact induced deformations near a contact-point and a dynamically growing crack-tip in soda-lime glass are demonstrated in this work. This second of a two-part paper demonstrates the applicability of DGS for the problems under stress wave loading conditions. Ultrahigh-speed photography (1 million frames per sec) in conjunction with DGS and a Hopkinson pressure bar to load soda-lime glass specimens are employed. The optical measurements are postprocessed to obtain relevant engineering parameters and stress field ($\sigma_x + \sigma_y$) near dynamically loaded crack-tip, both while stationary and during propagation.

KEYWORDS

digital gradient sensing, dynamic fracture, digital image correlation, impact, soda-lime glass

1 | INTRODUCTION

Soda-lime glass is a common structural material that accounts for over 90% of manufactured glasses. Superior optical transparency, good scratch resistance, high stiffness and hardness, very high compression strength, excellent heat and chemical resistance are some of the many attractive features besides its low-cost, recyclability, sustainability, and architectural esthetics which make this glass popular in many engineering and structural applications. This brittle material, however, suffers from a major inadequacy namely a low fracture toughness presenting the possibility of catastrophic failure during service. In a few critical applications such as transparent armor where

projectile impact and resistance to shock/blast loading are most important, layered architectures made of both glasses and tough polymers are employed.¹ Thus, understanding the fracture behavior of glasses under dynamic loading conditions is important for many life critical applications such as blast protectors, automotive windshields, transparent skyscraper cladding, etc.

Given its low fracture resistance, failure of glass is generally catastrophic and involves dynamic crack growth at very high speeds leading to branching and fragmentation. The underlying mechanics of these interconnected and intricate phenomena are yet to be fully understood. Performing full-field, noncontact measurement of deformations and stresses to evaluate various fracture parameters during

such high-speed events in brittle solids are highly beneficial to mechanical design but are rather challenging to do so because of severe spatial and temporal resolution requirements. For instance, longitudinal wave speed in soda-lime glass is ~ 5450 m/s with crack speeds exceeding 1500 m/s makes it difficult to implement full-field optical techniques easily.^{2,3} Additional challenges such as extremely small, highly localized region of intense deformations due to cracks that are almost mathematically sharp pose difficulties to measurement methods. Hence, most reported works on glasses²⁻⁵ have often relied on direct imaging of crack growth using high-speed photography coupled with postmortem inspection of fracture surfaces and crack growth morphologies. Acoustic emissions from a dynamically growing crack in a glass plate are used by some investigators⁶ to estimate surface displacements. Reports on quantitative full-field measurement near dynamically loaded stationary or growing cracks in glass are very few in the current literature directly attributable to the spatio-temporal challenges posed by the material. Legacy techniques of dynamic fracture such as photoelasticity have not been successful due to a relatively weak birefringence and low failure strain ($\sim 0.1\%$) displayed by soda-lime glass. The work of Takahashi et al⁷ is an exception; they have introduced a setup for high-speed photoelastic color photography to *qualitatively* observe dynamic fracture patterns in zone-tempered soda-lime glass. Pulsed laser assisted holographic interferometry using Q-switched ruby laser has been used in⁸ to visualize deformations and fracture of float glass subjected to stress waves in a shock tube. Optical method of caustics (or shadow spot method) has been employed to study dynamic fracture of tempered glass by Aratani et al⁹ They have reported dynamic stress intensity factors before and after crack branching by photographically monitoring the diameter of the shadow spot.

The sparse literature on this topic is indicative of the challenges associated with studying stress wave driven crack initiation and growth behaviors in glasses. The lack of a suitable, easy to implement, full-field, noncontact optical technique to study glasses (and ceramics in general) has been somewhat striking and needs attention. In this context, this work examines the feasibility of a full-field optical technique called digital gradient sensing (DGS)¹⁰ to tackle the stated problem. In DGS the elasto-optic effects exhibited by transparent soda-lime glass subjected to nonuniform state of stress are quantified by evaluating the angular deflections of light rays propagating through the material. The angular deflection measurements represent two orthogonal in-plane stress gradients under plane stress conditions. The presence of stress singularity at an impact point or a crack-tip makes DGS highly effective not only for mechanical field measurements but for locating the stress riser precisely. Authors have previously reported dynamic fracture

studies on transparent polymers¹¹⁻¹³ demonstrating the efficacy of DGS to study both mode-I and mixed-mode fracture problems. The current work is an attempt to extend it to study extremely brittle material such as soda-lime glass. As noted earlier, the angular deflections produced in glass are extremely small and hence typical experimental parameters had to be altered to tackle this challenge.

In the first part¹⁴ of this two-part paper, the feasibility of DGS to study quasi-statically loaded contact stress problem and crack-tip problem has been demonstrated. In this second part, two different experiments under impact loading are reported to demonstrate the feasibility of DGS for performing accurate and reliable dynamic measurements in soda-lime glass. First, stress concentration due stress wave loading conditions using a Hopkinson pressure bar apparatus and ultrahigh-speed photography on a soda-lime glass is studied. Next, deformations near a dynamically loaded crack-tip are studied. The experimental measurements performed are comparatively evaluated independently using boundary/far-field measurements and complimentary finite element analysis, respectively. The results are summarized at the end of the report.

2 | WHY NOT USE 2D DIC TO STUDY FRACTURE IN SODA-LIME GLASS?

Aided by advances in digital photography, image processing algorithms, and abundance of inexpensive computational power, the digital image correlation method (or simply DIC) has emerged as a popular optical metrology tool¹⁵ in recent years. Easy specimen preparation, ordinary white light illumination requirements, and accessibility of results in the digital form have all added to its popularity as well.

Considering authors' previous works on dynamic fractures in brittle polymers and composites,^{16,18} the possibility of using DIC to study fast fractures in glass was considered first to address the problem. Accordingly, experiments were performed on a soda-lime glass specimen using 2D DIC. The geometry and loading configuration of soda-lime glass plate specimens that were used are shown in Figure 1A. The specimen surface was coated with random black and white speckles. It was dynamically loaded using a Hopkinson pressure bar with a wedge-shaped tip placed in contact with the matching V-notch machined into the specimen. A photograph of the fractured specimen is shown in Figure 1B. The crack initiated at the prenotch and propagated under dominant mode-I conditions before bifurcating into two globally near-symmetric daughter cracks approx. in the middle of the specimen. This highly transient event was recorded using a single sensor Kirana-05M ultrahigh-speed

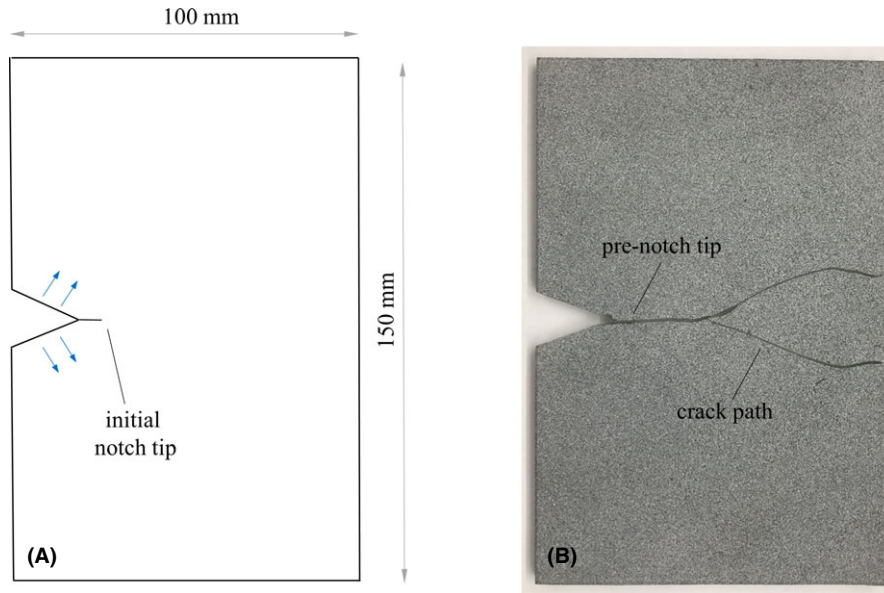


FIGURE 1 (A) Specimen geometry and loading configuration used in the study of soda-lime glass fracture using 2D-DIC, along with (B) the photograph of the fractured specimen [Color figure can be viewed at wileyonlinelibrary.com]

camera (924×768 pixels; scale factor = 0.072 mm/pixel) at 1 million frames per second. The magnification selected here was dictated by the need for observing a sufficiently large region (approx. 64 mm \times 53 mm) on the specimen to capture crack initiation, growth, and branching events (further, this region-of-interest was comparable to that used to study dynamic fracture using DGS, to be described later).

The fracture event produced a hair-line crack emanating from the prenotch-tip but could not be discerned directly from the recorded speckle images. This is unlike the polymeric and fiber reinforced composite material counterparts previously studied successfully by the authors' group^{16–18} where the crack path and the tip were often visible and/or easily detectable in the recorded images. This disparity in the visibility of the crack-tip within the recorded speckle images between a relatively compliant brittle polymers and stiff soda-lime glass is shown in Figure 2. Figure 2A

shows a speckle image at $t = 26 \mu\text{s}$ ($t = 0 \mu\text{s}$ represent crack initiation at original notch-tip) for soda-lime glass and Figure 2B is an epoxy counterpart in a mode-I fracture experiment¹⁶ previously reported by the authors' group. A visual inspection of the images does not reveal the presence of a crack in the former, when in reality the crack has indeed propagated beyond the center of the image. On the other hand, the propagating crack-tip is readily visible in the latter case even without any processing. This difficulty can be further understood better by enumerating the expected crack flank displacements in these two cases. In soda-lime glass, based on LEFM, it can be shown that it is in the submicrometer(nano) scale even at 3 to 4 mm from the crack-tip. On the contrary, the same for epoxy is ~ 100 micrometers, which is relatively easy to detect.

Using the image analysis software ARAMIS[®] (GoM GmbH, Braunschweig, Germany), speckle images in the deformed and undeformed states were correlated and

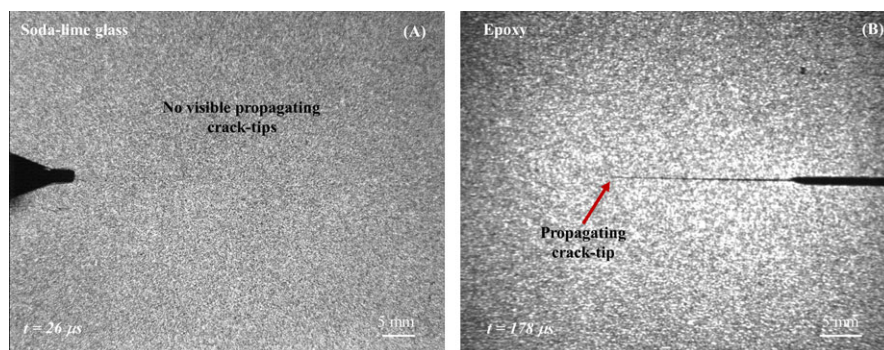


FIGURE 2 Speckle images recorded during mode-I dynamic fracture of (A) soda-lime glass and (B) epoxy specimens. The location of the propagating crack-tip is readily visible in the latter but not in the former due to crack flank displacement of the order of 100 microns vs submicrometer in glass

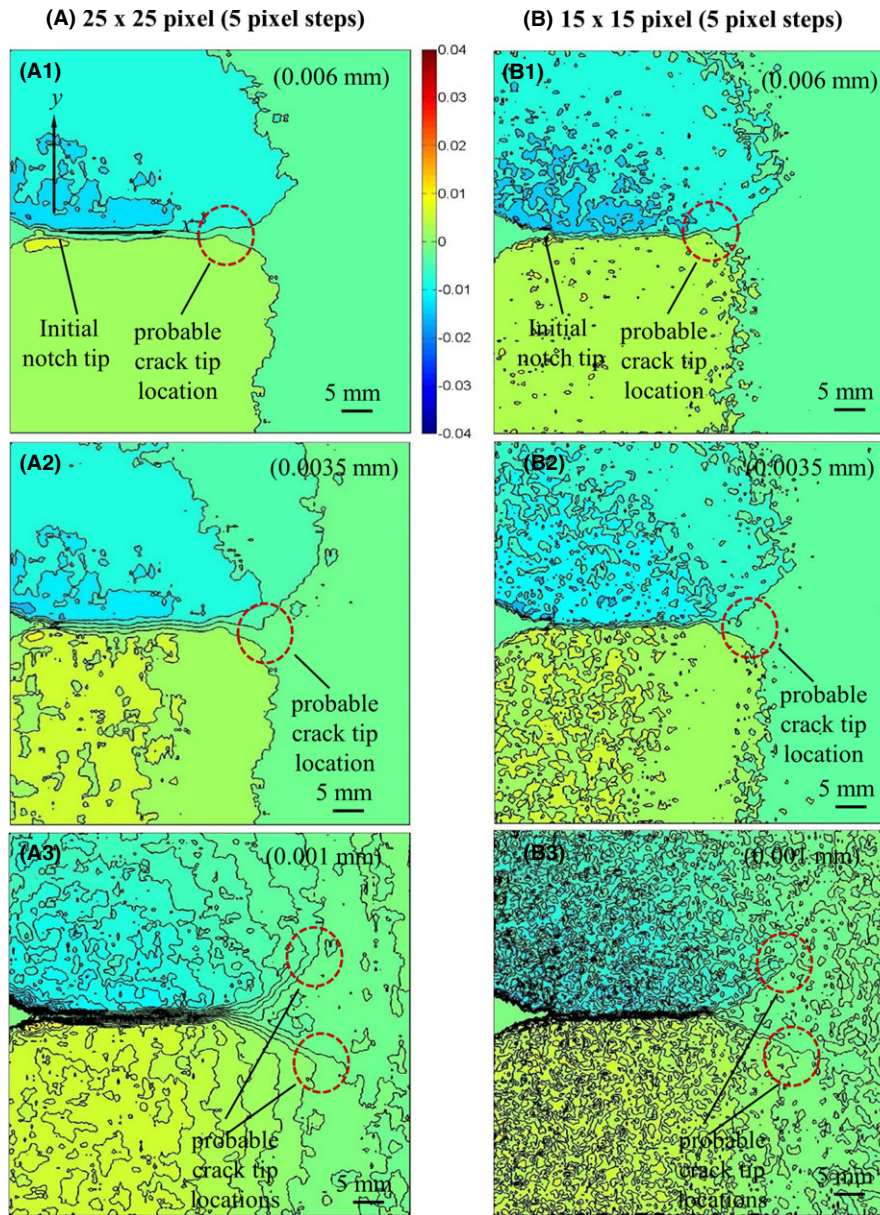


FIGURE 3 Displacement contours on soda-lime glass specimen surface along the vertical direction (normal to the crack) from DIC at a time instant of $\sim 26 \mu\text{s}$ after crack initiation at the original tip using sub-image size of (A) 25×25 pixel, and (B) 15×15 pixel with step size of 5 pixels with contour increments of 0.006 mm, 0.0035 mm, and 0.001 mm ((A1)-(A3) and (B1)-(B3) respectively) [Color figure can be viewed at wileyonlinelibrary.com]

in-plane deformations were obtained. Two typical subimage sizes of 25×25 pixels and 15×15 pixels with step size of 5 pixels were used while analyzing the images. The resulting displacement contours in the vertical direction (perpendicular to the crack growth direction) are plotted using three different contour increments, 6 μm to 1 μm , in Figure 2A,B. As the magnitude of contour increments was decreased (the 1 μm increment being close to the limit of DIC for the chosen experimental parameters) for visualization, the probable location of the crack-tip varied significantly between Figure 3A1,A2 and quite drastically between Figure 3A2,A3. In fact, the first two figures suggest a single

(growing) crack-tip whereas the last one indicates a fully bifurcated crack with two branched crack-tips. Similar observation can be made from Figure 3B1-B3 as well. Thus, locating the crack-tip could be quite challenging in this very brittle material where crack flank displacements are extremely small compared to polymers and fiber reinforced composites. If the crack-tip is located incorrectly, the fracture parameters (velocity and stress intensity factor) thus evaluated will be incorrect as well. This difficulty could be alleviated if a higher magnification is used. However, it would require substantial compromise in terms of the region-of-interest being investigated, possibly missing different

fracture mode transitions and mechanisms that occur during such a highly transient event.

Considering the above raised concerns with 2D DIC to study dynamic fracture of glass, it is also worth noting a few advantages (and disadvantages) of DGS method described in the part-I of this article (¹⁴ see Figure 1). Briefly, the transmission-mode DGS is a full-field optical method that leverages 2D DIC *along with* the elasto-optic effect exhibited by transparent materials to measure small angular deflections of light rays produced by the combined effect of refractive index and thickness changes due to stresses in them. The measured angles are proportional to the spatial gradients of $(\sigma_x + \sigma_y)$ where σ_x, σ_y are the in-plane normal stresses in Cartesian coordinates.¹⁰

The benefits of using DGS to study dynamic fracture of glass are as follows: First, the measurement sensitivity can be easily changed in DGS by simply modifying the distance (or, the ‘optical lever’) between the specimen and the ‘speckle target’—a planar surface with the desired speckle decoration placed parallel to and behind the specimen (see, part-I of this paper¹⁴). This makes it possible to investigate brittle materials such as glass which exhibit extremely small thickness and refractive index changes due to high stiffness and low toughness by simply increasing the distance between the specimen and the ‘target’. Second, an important advantage of DGS is that when studying stress concentration problems involving a moving damage front such as a rapidly growing crack, where locating the instantaneous crack-tip is critical for extracting the fracture parameters correctly. Being a stress gradient measurement technique, mechanical fields from DGS, say visualized as contours of orthogonal angular deflection components, converge to the crack-tip location. This greatly helps to identify the spatial position of the singularity in the region-of-interest and is unlike 2D-DIC due to the nonsingular nature of the measured mechanical fields.* Third, the availability of orthogonal stress gradients in DGS as a rectangular array of data lends itself to an easy implementation of 2D integration schemes to estimate stresses²² making it an alternative to very few techniques capable of measuring stresses. Lastly, unlike other DIC techniques, here the specimen does not require speckle decoration. Instead, the same ‘target’ with the desired speckle decoration can be used repeatedly in multiple experiments without introducing variability to the gauging pattern between experiments. This reduces experimental effort needed for creating consistent speckle decoration with identical characteristics.

*Often locating the crack-tip is done using its visibility among random speckles in the recorded images¹⁶ and/or displacement jump across the crack flanks in polymers, metals and composites. When it fails, other sophisticated methods such as nonlinear least-squares regression with crack-tip position as an unknown,¹⁹ genetic algorithms,²⁰ subset splitting approach,²¹ to name a few, are needed. These approaches are computationally very expensive due to the addition variables and numerical convergence is not always assured.

The disadvantages of *transmission-mode* DGS method include: (i) the need for the specimen to be transparent,[†] (ii) the salient specimen features such as edges, cracks are often blurry or not readily visible in the recorded images as the speckle target behind the specimen is being focused on and it becomes evident only upon completing the image correlation.

In light of the above discussion on the pros and cons of DGS, the method has a few distinct advantages which are beneficial to study the problem in hand and will be discussed next.

3 | DYNAMIC LINE-LOAD ON THE EDGE OF A SHEET (EDGE-ON-IMPACT)

3.1 | Experimental details

First, the contact stresses due to a dynamically applied line-load on the edge of a planar soda-lime glass sheet were studied using DGS. Impact loading apparatus was used to load the sample and DGS in conjunction with ultra-high-speed photography was used for optical metrology.

The schematic of the experimental setup is shown in Figure 4. A $75 \times 100 \text{ mm}^2$ rectangular glass plate of thickness 5.65 mm was used for this experiment. The specimen was placed on a 2 mm thick strip of soft putty stuck to a height-adjustable micro-positioning device and subjected to dynamic line-load using a Hopkinson pressure bar as shown in Figure 5. Another strip of putty was placed on the top of the specimen to create symmetry in boundary conditions about the loading axis. The Hopkinson bar apparatus consisted of an AL 7075-T6 long-bar (1.83 m long, 25.4 mm diameter) with a cylindrical head pushed against the long edge of the specimen. The long-bar was impacted by propelling a ~ 305 mm long, 25.4 mm diameter AL 7075-T6 striker placed within the barrel of a gas-gun aligned coaxially with it.

A Kirana model-05M ultrahigh-speed digital camera equipped with a single sensor of 924×768 pixels (10-bit gray scale resolution) capable of acquiring 180 images was used for recording the dynamic impact event. The speckles on the target plane were illuminating using two high-energy flash lamps (Cordin model 659). Other experimental parameters such as the trigger delay, flash duration, framing rate, and image storage were all controlled using a standalone computer. A Nikkor 80-400 mm focal length macro zoom lens along with a focal length doubler (2X teleconverter) and an adjustable bellows were used for imaging the speckles from a distance. Furthermore, an aperture setting of $F^{\#}11$ was used to achieve a good exposure and a sharp focus during high-speed imaging. The camera was at 2362 mm in front of the specimen. A target

[†]For opaque materials, the *reflection-mode* DGS can be employed.²³

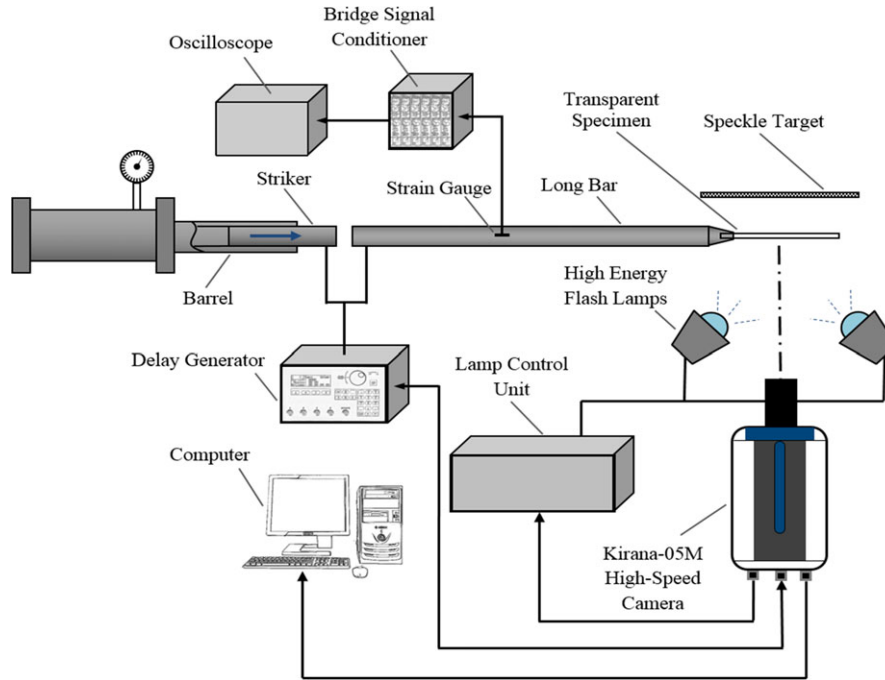


FIGURE 4 Experimental setup (top view) used to study the edge-on impact and the dynamic fracture of soda-lime glass [Color figure can be viewed at wileyonlinelibrary.com]

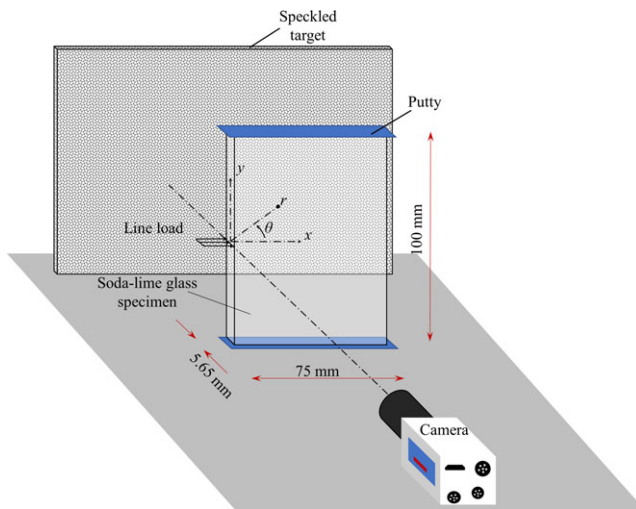


FIGURE 5 Schematic of the specimen loading configuration used to measure deformations due to dynamically imposed line-load on the edge of a soda-lime glass specimen (using a Hopkinson bar) [Color figure can be viewed at wileyonlinelibrary.com]

plate coated with random black and white speckles was placed 1222 mm behind the specimen from the mid-plane of the specimen. A couple of black dots were marked on the target to relate the image dimensions to the actual target dimensions. The region-of-interest in this study was around the contact-point between the long-bar and specimen. Hence, the camera was focused on a rectangular region of 125 mm × 102 mm on the target plate (or approx. 85 × 67 mm² region on the specimen plane)

around the contact point. Care was exercised to achieve a near-Gaussian distribution of gray scales by adjusting the location of the flash lamps iteratively. The loading event was initiated by discharging compressed air in the gas-gun cylinder that propelled the striker placed inside the barrel. When the moving striker impacted the long-bar, it initiated a compressive stress wave that traveled the length of the bar before imparting a transient line-load to the specimen. The duration of the loading phase of the pulse generated was ~120 μs (see Figure 13 inset). Also, a trigger pulse was generated when the striker contacted the long-bar which initiated recording of the speckles by the camera at 1 million frames per second with a 320 μs delay. The delay was selected based on the excursion time for the stress waves to travel the length of the long-bar before loading the sample. A trigger pulse from the camera operated the flash lamps. A strain gage affixed to the long-bar measured the strain history that was later used to determine the contact force history on the specimen. The time delay initiated the camera recording well in advance of the start of the loading event. This ensured capturing a few ‘reference images’ (speckle images when there is no deformation in the specimen) to be used during image correlation to be performed later. Thus, a total of 180 images were recorded at 1 μs intervals between successive images with about 10-20 images ahead of the loading phase. Using one of these images as the reference image, the entire series of deformed images were correlated to obtain the angular deflections in the region-of-interest.

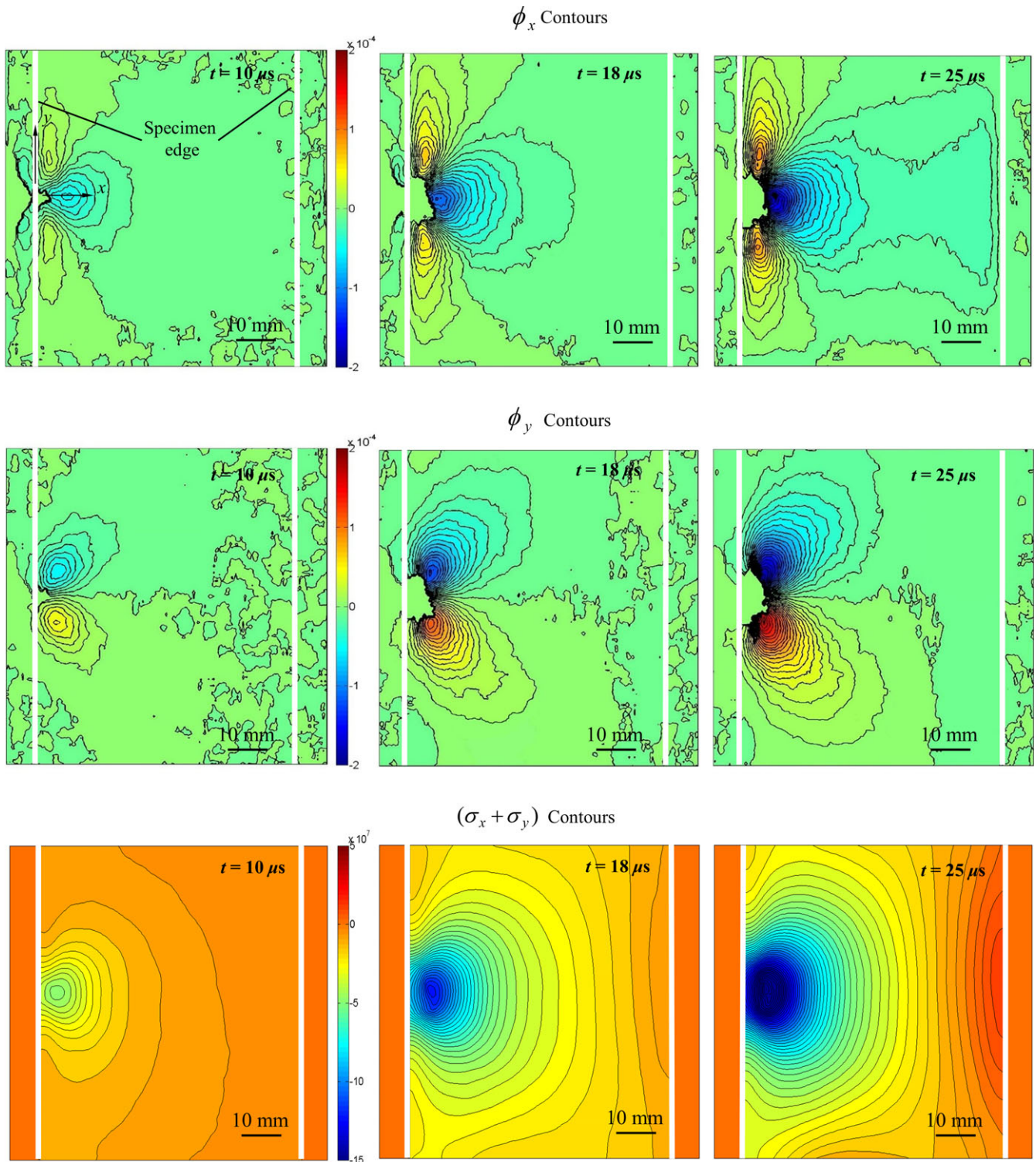


FIGURE 6 Angular deflection contour plots (contour interval = 8×10^{-6} rad) proportional to stress gradients of $(\sigma_x + \sigma_y)$ in the x - (top row) and y -directions (middle row) for a soda-lime glass specimen subjected to dynamic line-load on its edge. The corresponding numerically integrated stress gradients representing contours of stress $(\sigma_x + \sigma_y)$ are shown in the bottom row (contour interval = 4 MPa)[Color figure can be viewed at wileyonlinelibrary.com]

The images were correlated using ARAMIS[®]. Each image was segmented into facets/sub-images consisting of 25×25 pixels during analysis. An overlap of 20 pixels (ie, step size of 5 pixels) was used during image

analysis. This resulted in a matrix of 146×177 data points in the region of interest for each of the two orthogonal angular deflection fields. In-plane orthogonal deflections were subsequently evaluated using the

known distance Δ between the specimen and the target planes.

3.2 | Evaluation of load history

For evaluating the dynamic load history due to impact, the problem was approximated as a line-load imposed on the edge of an infinitely large plate. This assumption allowed using Flamant-like stress field,¹⁴

$$\phi_{x,y}(t) = \pm C_{\sigma} \frac{2F(t)}{\pi} \frac{[\cos(2\theta); \sin(2\theta)]}{r^2} \quad (1)$$

The instantaneous force, $F(t)$, was evaluated using over-deterministic least-squares analysis of the measured $\phi_x(t)$ fields. The coordinates of the target plane were mapped to the specimen plane during analysis. Discrete angular deflection values around the loading point in the region $1 \leq r/B \leq 2$ along with angular extent of $-80^\circ \leq \theta \leq -50^\circ$, $-40^\circ \leq \theta \leq 40^\circ$ and $50^\circ \leq \theta \leq 80^\circ$ were used in the least-squares analysis. This ensured the elimination of regions of dominant stress triaxiality near the loading point. This also helped to avoid data along the free edges and regions where angular deflections are nearly zero. It should be noted that in Equation (1), rigid body motions ($C_{x,y}$ in Equation (3) of part-1) are negligible as stress wave dominant events last less than 100 μ s.

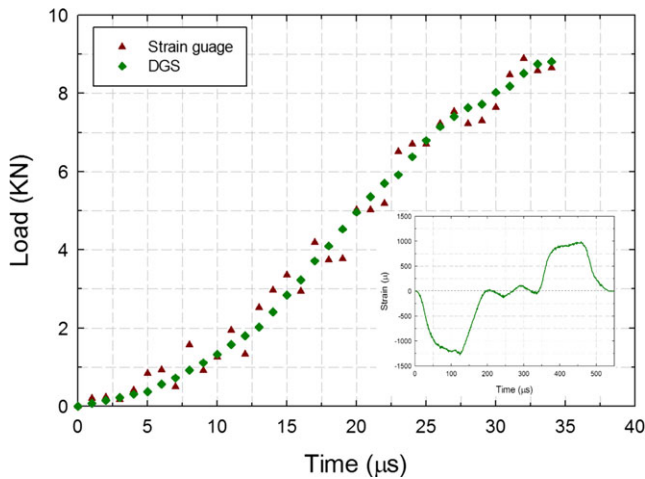


FIGURE 7 Compressive load history measured using digital gradient sensing data near the impact point (green diamonds); Force history extracted from strain gage measurements on the long-bar (red triangles). Inset shows the strain history measured on the long-bar [Color figure can be viewed at wileyonlinelibrary.com]

Using the strain gage affixed on the long-bar of the Hopkinson loading setup, strain history was recorded throughout the experiment (see Figure 7 inset). Load history was evaluated from the strain history as,¹⁰

$$F(t) = E_b A_b (\epsilon_I(t) + \epsilon_R(t)) \quad (2)$$

where, E_b (~ 70 GPa) and A_b (506.7 mm^2) are the elastic modulus and cross-section area of the long-bar, respectively. Strains ϵ_I and ϵ_R denote incident and reflected strain signals.

3.3 | Experimental results

The measured DGS contours (on the specimen plane) of angular deflections ϕ_x and ϕ_y for three select time instants are shown in Figure 6. It should be noted that the contours near the free edge of the specimen show unavoidable edge effects due to finite subimage size. Also, shown in Figure 6 are numerically integrated stress gradients represented as contours of $(\sigma_x + \sigma_y)$ using a higher order finite-difference-based least-squares integration (HFLI) scheme demonstrated in Ref.²² Evidently, the smoothing effect of the integration scheme on the measured data (in rows 1 and 2) is readily visible in these contours with all the essential features associated with the edge-on-impact of a finite plate fully preserved. That is, the impact region shows a concentration of nearly semicircular compressive stress contours at the early time instant (10 μ s) without significant stresses at the opposite free-edge. At later time instants, say, at 25 μ s after impact, the stress concentration at the impact point has intensified as evident from the increased contour density and the reflected stress waves at the free-edge have turned tensile with contours nearly parallel to the specimen edge. Figure 7 shows the plot of measured load histories from the strain gage along with that from the optical (DGS) data analysis. The load history extracted from DGS measurements is in good agreement with that obtained from the strain gage.

4 | DYNAMIC CRACK-TIP DEFORMATIONS

4.1 | Experimental details

The problem of a dynamically loaded stationary and rapidly growing mode-I crack was studied next using DGS and ultra-high-speed photography. The experimental setup used is same as that described in the previous section (Figure 4). The Hopkinson pressure bar (long-bar) was used to subject a soda-lime glass specimen to reverse impact loading. The long-bar was a 1.83 m long steel cylindrical bar of 25.4 mm diameter with a tapered rectangular tip ($25.4 \text{ mm} \times 6.7 \text{ mm}^2$) pushed against an unconstrained 150 mm \times 100 mm rectangular single-edge-notch (SEN) specimen. A 305 mm long, 25.4 mm diameter rod held inside the barrel of a gas-gun was coaxially aligned with the long-bar and was used as the striker. Both the long-bar and the striker-bar were made of maraging steel eliminating any impedance mismatch between them. The soda-lime glass

sample had an initial edge notch of 12 mm length and 300 μm thickness that originated from one edge. The sample was loaded symmetrically relative to the initial notch to initiate and propagate a mode-I crack. Figure 8 shows the schematic of the specimen geometry and loading configuration.

During the dynamic fracture event, the speckles on the target were recorded using a Kirana 05M camera assisted by a pair of high energy flash lamps illuminating the target. The rest of the details are same as that detailed in the previous section. The region-of-interest in this part of the study was around the initial notch-tip. The camera was focused on a 93 mm \times 77 mm region on the target plate (approx. 62 \times 51 mm² region on the specimen plane) through the vicinity of the initial notch-tip. At the start of the experiment, the striker was launched toward the long-bar using the gas-gun. When the striker contacted the long-bar, a compressive stress wave was generated in the long-bar, which propagated along its length before loading the specimen over a small rectangular area associated with the tapered long-bar tip (contact area \sim 5.6 mm \times 6.7 mm). The duration of the loading phase of the pulse generated was \sim 125 μs . When the striker contacted the long-bar, a trigger signal was also generated. This initiated recording of images at 1 million frames per second at a preset delay of 380 μs . The delay was set such that the camera started recording images well in advance of the start of loading so that a few reference images were available for subsequent correlation of speckle images in the deformed state with the one from the undeformed or reference state. A total of 180 images were recorded at 1 μs intervals, with 10-20 images well before the sample started to experience stress waves. Using one of the images before loading as the reference image, the entire series of recorded images were correlated to obtain instantaneous angular

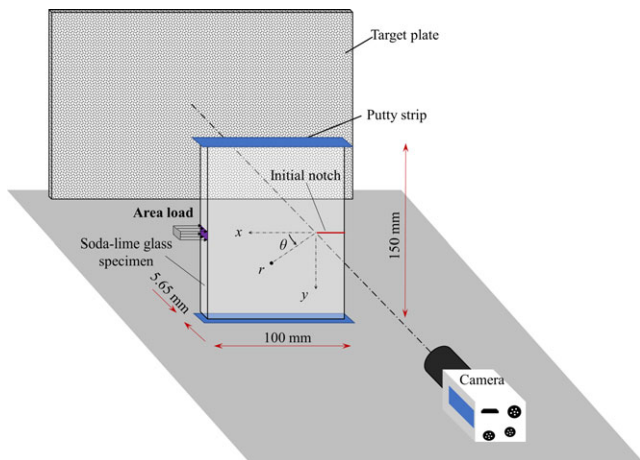


FIGURE 8 Schematic of the specimen loading configuration used in reverse impact fracture experiments on soda-lime glass. The load was imposed using a Hopkinson bar making an area contact with the specimen edge

deflections at 1 μs intervals. The recorded image corresponds to approximately 62 \times 51 mm² region of the specimen plane (note that this region on the specimen plane is comparable to the one used for DIC measurements, Figure 1). Each image was segmented into facets/subimages consisting of 25 \times 25 pixels during analysis. An overlap of 20 pixels (ie step size of 5 pixels) was used during image correlation. This resulted in a matrix of 146 \times 177 data points in the region-of-interest for each of the two orthogonal angular deflection fields. Subsequently in-plane orthogonal deflections were evaluated using the known distance Δ between the specimen and the target planes.

4.2 | Crack velocity and stress intensity factor (SIF) histories

The position of the crack-tip determined from the angular deflection fields at each instant was used to measure the instantaneous crack length. Subsequently, the crack velocity (V) was estimated from the crack length history using backward difference method. The mapping function¹⁴ was taken into consideration during the analysis to obtain both velocities and SIFs. The mode-I and mode-II SIFs were evaluated from an over-deterministic least-squares analysis of the crack-tip data in conjunction with the asymptotic equation (See¹¹ for details) with $N = 4$. In case of a propagating crack-tip the following crack-tip field,

$$\phi_x(t) = C_{\sigma B} \left[\begin{array}{l} -\frac{1}{2}r^{-\frac{3}{2}} \left\{ f(V; C_L; C_S)A_1(t) \cos\left(\frac{3\theta}{2}\right) \right. \\ \left. + g(V; C_L; C_S)D_1(t) \sin\left(-\frac{3\theta}{2}\right) \right\} \\ + \sum_{N=2}^{\infty} \left\{ A_N(t) \left(\frac{N}{2}-1\right) r^{\left(\frac{N}{2}-2\right)} \cos\left(\left(\frac{N}{2}-2\right)\theta\right) \right. \\ \left. + D_N(t) \left(\frac{N}{2}-1\right) r^{\left(\frac{N}{2}-2\right)} \sin\left(\left(\frac{N}{2}-2\right)\theta\right) \right\} \end{array} \right] \quad (3)$$

was used. In the above, f and g are functions of instantaneous crack velocity V and (r, θ) denote the contracted crack-tip polar coordinates. Further, (r, θ) can be expressed in the local Cartesian coordinates moving with the crack-tip (x, y) as, $r = \left\{ (x)^2 + \alpha_L^2(y)^2 \right\}^{1/2}$ and $\theta = \tan^{-1}\left(\frac{\alpha_L y}{x}\right)$. The coefficients of $A_1(t)$ and $D_1(t)$ in the asymptotic series are related to the mode-I and mode-II stress intensity factors $K_I(t)$ and $K_{II}(t)$, respectively, as $A_1(t) = K_I(t) \sqrt{2/\pi}$ and $D_1(t) = K_{II}(t) \sqrt{2/\pi}$. The functions f and g are,

$$f(V; C_L, C_S) = \left(\frac{1+\nu}{1-\nu} \right) \frac{(1+\alpha_S^2)(1-\alpha_L^2)}{4\alpha_L\alpha_S - (1+\alpha_S^2)^2}, \text{ and} \quad (4)$$

$$g(V; C_L, C_S) = \left(\frac{1+\nu}{1-\nu} \right) \frac{2\alpha_S(1-\alpha_L^2)}{4\alpha_L\alpha_S - (1+\alpha_S^2)^2}$$

where $\alpha_L = \left[1 - \frac{\rho(1-\nu)}{2\mu} V^2 \right]^{\frac{1}{2}}$ and $\alpha_S = \left[1 - \frac{\rho}{\mu} V^2 \right]^{\frac{1}{2}}$ for plane stress, with μ and ρ being shear modulus and mass density respectively. Data in the region $0.5 \leq r/B \leq 1.5$

along with angular extent of $-150^\circ \leq \theta \leq 150^\circ$ near the crack-tip were used for analysis. Note that, Equations (3) and (4) can be reduced to the form of a dynamically loaded stationary crack in the limit the crack velocity $V \rightarrow 0$.

4.3 | Finite element simulation

Complementary elasto-dynamic finite element simulations of reverse impact induced mode-I deformations in SEN soda-lime glass specimen was carried out using ABAQUS®/Explicit structural analysis software. The specimen and loading configuration are shown in Figure 8. The long-bar (Hopkinson bar) in the loading setup was also modeled for performing this simulation. The impact end of the long-bar was rectangular as in the experiments and made an area contact with the specimen. The model consisted of 64 226 and 563 509 solid 3D tetrahedral elements respectively. The discretized model with the crack opening displacements is shown in Figure 9A. The time steps during the analysis were allowed to be automatically controlled by the time-integration scheme. Table 1 shows the material properties of soda-lime glass and the maraging steel long-bar used in the simulation. The particle velocity obtained from strain gage readings (see Figure 9B) on the Hopkinson pressure bar experiment was input into the analysis. The instantaneous crack opening (v) and sliding (u) displacements were extracted along the two crack faces. This was repeated for each time step. The apparent mode-I and mode-II stress intensity factors (SIFs), $(K_I)_{app}$ and $(K_{II})_{app}$ at each step were computed using,¹³

$$(K_{I;II})_{app} = \frac{E\sqrt{2\pi}}{8\sqrt{r}}(v; u); (r, \theta = \pi) \quad (5)$$

Using linear regression on these apparent SIFs, the instantaneous SIFs ($K_I(t)$ and $K_{II}(t)$) were obtained.

4.4 | Experimental results

The two orthogonal angular deflection fields ϕ_x and ϕ_y (on the specimen plane) at three select time instants are shown in Figure 10. They correspond to a time instant before crack initiation ($t = -4 \mu\text{s}$), at crack initiation ($t = 0 \mu\text{s}$) and during mode-I crack growth ($t = +4 \mu\text{s}$). As expected, the two orthogonal angular deflection fields representing stress gradients in the direction along and perpendicular to crack growth are symmetric and antisymmetric, respectively, relative to the mode-I crack plane. Also, as noted at the beginning of this article, locating the tip of a hairline crack in soda-lime glass is quite challenging when random speckles are present in the images. However, locating the same after image correlation is simpler due to the singular nature of the crack-tip field measured by DGS. That is, in each of these images the crack-tip location can be

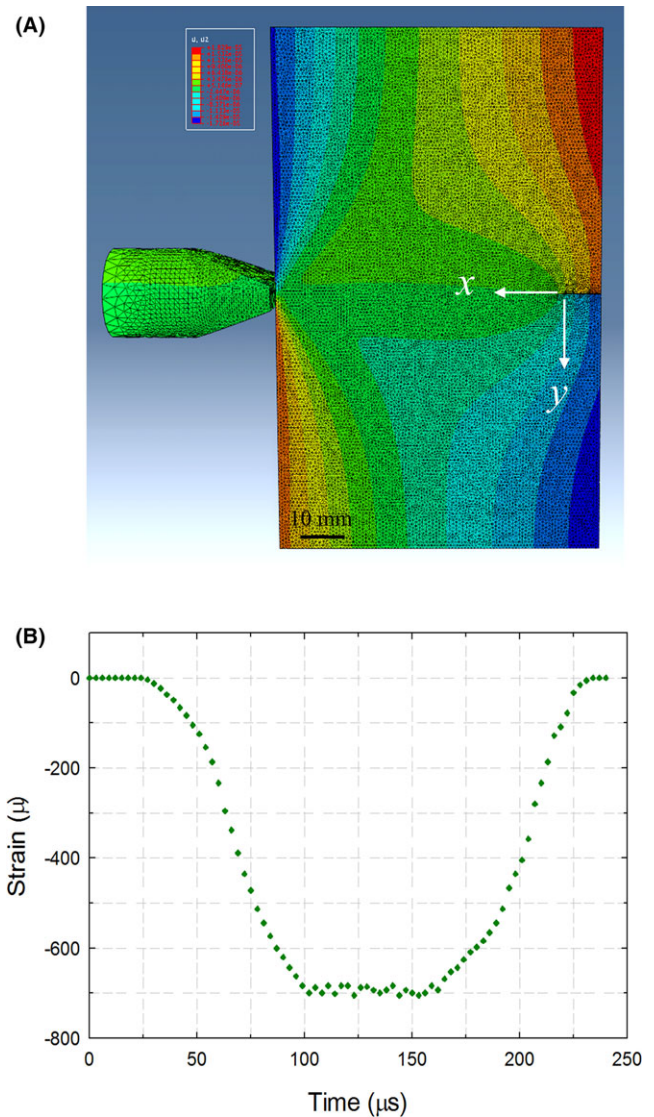


FIGURE 9 (A) Discretized finite element model of SEN soda-lime glass specimen subjected to dynamic edge loading with an overlay of displacements in the y-directions. (B) The strain history recorded on the Hopkinson bar used as input into the FE simulation [Color figure can be viewed at wileyonlinelibrary.com]

TABLE 1 Dynamic material properties of maraging steel and soda-lime glass used for FE simulation

Parameter	Maraging steel	Soda-lime glass
Density	8000 kg/m ³	2500 kg/m ³
Elastic modulus	200 GPa	70 GPa
Poisson's ratio	0.3	0.22

identified easily by making use of singular nature of the two orthogonal stress gradients along with symmetry or antisymmetry requirements for each field. The change in the contour sign along the x- and y-axes in these fields is very helpful in this regard. Also, shown in Figure 10 are numerically integrated values of stress gradients resulting

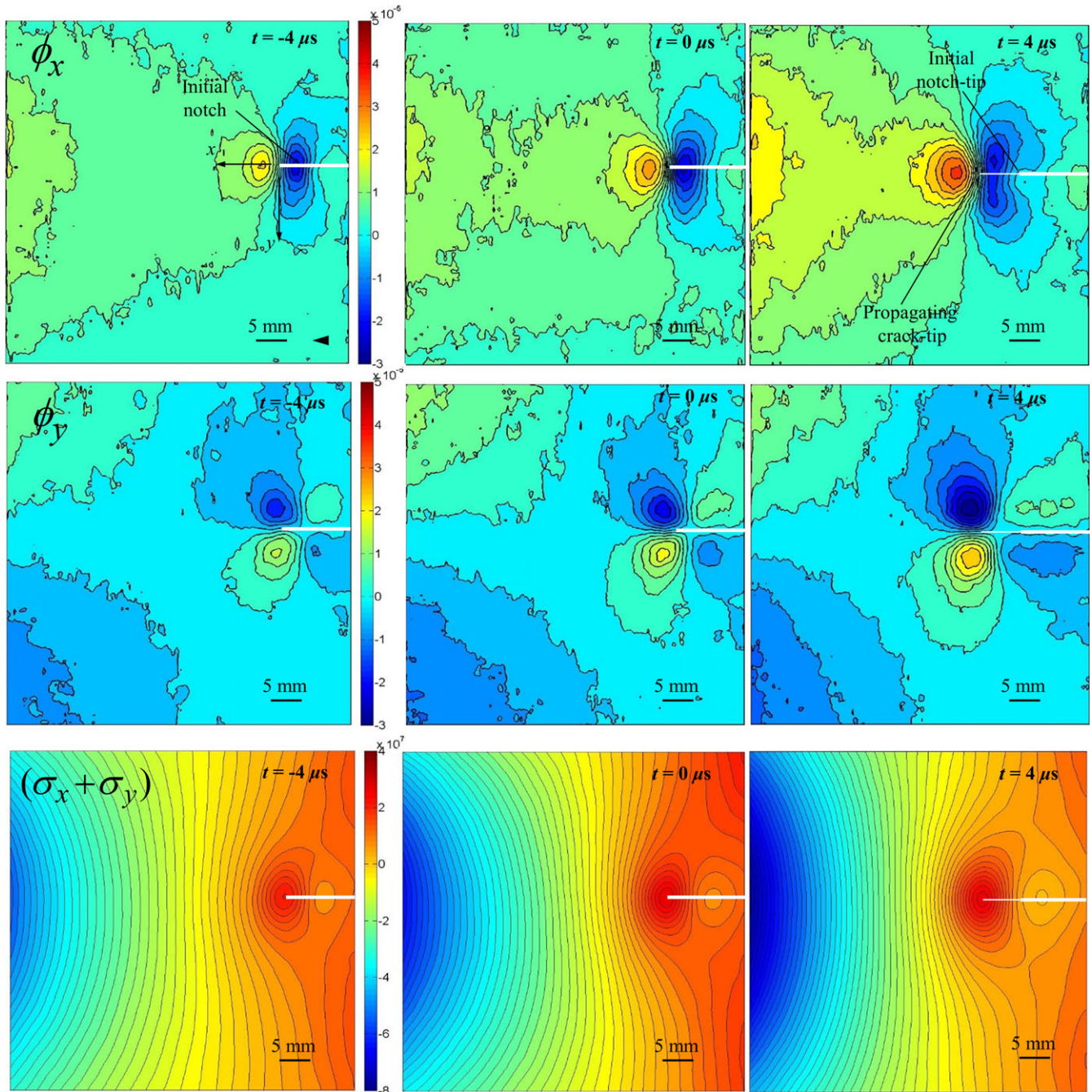


FIGURE 10 Angular deflection contour plots (contour interval = 4×10^{-6} rad) for a soda-lime glass SEN specimen subjected to dynamic edge loading along with the first stress invariant (contour interval = 2 MPa) obtained by integrating the digital gradient sensing data using higher-order finite-difference-based least-squares integration. The arrowhead shows the crack growth direction (Note that $t = 0 \mu\text{s}$ in these correspond to the crack initiation at original notch tip) [Color figure can be viewed at wileyonlinelibrary.com]

in contours of $(\sigma_x + \sigma_y)$ using a HFLI scheme demonstrated in Ref.²² Evidently, the smoothing effect of the integration scheme on the measured data (in rows 1 and 2) is visible in these contours with all the essential features associated with the crack growth phenomenon in a finite plate fully preserved. That is, the left-hand edge of the sample being impact loaded by the long-bar produces compressive stress waves as evident from the negative contour values

adjacent to left vertical edge of the images.[‡] The right edge of the plate containing the initial notch shows positive stress contours hugging it, again consistent with the reflected compressive stress waves turning tensile upon reflection at the vertical free-edge. Furthermore, the crack-

[‡]Note that the region-of-interest in these recordings precluded impact point and hence not visible.

tip is surrounded by bean shaped (epicycloids) positive (tensile) contours expected for $(\sigma_x + \sigma_y) (\propto f(V) K_I(t) r^{-1/2} \cos(\theta/2))$ based on linear elastic fracture mechanics.

Figure 11 shows the crack velocity history for two different specimens (marked S1 and S2). The velocity histories for both the specimens essentially overlap on each other showing the repeatability of the experiments. It should be noted that the instantaneous crack-tip was located in each image after performing correlation with the reference image. The crack velocity increases from 0 to 1320 m/s within a few microseconds after initiation. Subsequently the crack reached a stable velocity of ~ 1450 m/s which is similar to that reported by Doll.³ This corresponds to a very high crack acceleration of approx. 3×10^8 N/m² (or 30×10^6 g). The photograph of the fractured surface in the steady crack growth region is shown as an inset in Figure 11. It can be seen that during the stable crack growth, the crack surface shows a “mirror” like finish.²⁴

The optical fields measured using DGS were analyzed using least-squares analysis to extract the SIFs before and after crack initiation. The SIFs have been evaluated by fitting Equations (3) and (4) discussed earlier to the measured $\phi_x(t)$ data shown in Figure 12 as a time history (the SIFs for two different specimens tested are overlaid). The good agreement between the SIFs for both the specimens shows a *high degree of experimental repeatability and robustness of the methodology to evaluate SIFs*. During the loading phase, the notch-tip experienced a SIF evolution consistent with the strain pulse generated during that phase (see, Figure 9B). The monotonic and rapid increase in $K_I(t)$ occurred until crack initiation ($t = 0$) whereas $K_{II}(t)$ remained nearly zero as to be expected in this mode-I

configuration. Ideally, $K_{II}(t)$ should be zero for a mode-I crack, hence the nonzero values of $K_{II}(t)$ can be considered as the error in the least-squares analysis of DGS data. The fracture toughness ($K_I(t)$ at $t = 0$) was recorded as 0.81 MPa \sqrt{m} . This value is higher than that reported for quasi-static loading conditions^{25,26} and lower than that reported for dynamic loading conditions.²⁷ However, it should be noted that various factors including notch tip radius and loading rate could alter the measured fracture toughness. The lower notch-tip radius (~ 150 μ m) used in this study could be a factor for observed lower fracture toughness under dynamic loading conditions.

At crack initiation ($K_I(t) \sim 0.81$ MPa \sqrt{m} ; $dK_I/dt \sim 1.5 \times 10^5$ MPa \sqrt{m}/s) there is a distinct dip in $K_I(t)$ history punctuating the dynamic unloading in the region of analysis. The postinitiation $K_I(t)$ values recover rapidly within a couple of microseconds and increase monotonically until the end of the observation window at progressively decreasing rates. The values of $K_{II}(t)$ in the postinitiation period also remain nearly zero suggesting that the crack was indeed traveling under dominant mode-I conditions. The comparison of the computed SIFs until crack initiation with the counterpart from finite element simulations are shown in Figure 13. It should be noted that the $K_I(t)$ value at crack initiation was forced to match with the experimental history in this comparison due to uncertainty in the time instant of impact and material properties of the bar and the specimen. A good agreement between the measured and computed values of SIFs can be seen all the way back to the early time instants where notch-tip starts to experience load.

From the instantaneous crack velocity V and mode-I SIF K_I in Figures 11 and 12, respectively, the dynamic energy release rates were evaluated as,²⁸

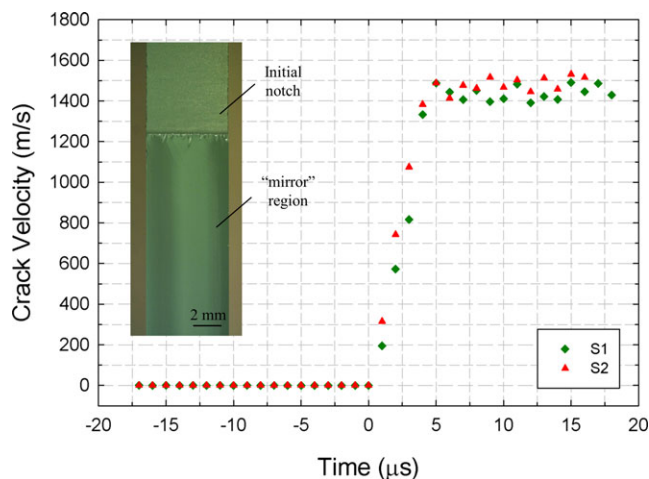


FIGURE 11 Velocity histories of propagating cracks from two different specimens, S1 and S2. Inset: photograph of the fractured surface of the specimen ($t = 0$ μ s corresponds to crack initiation at the original notch tip)

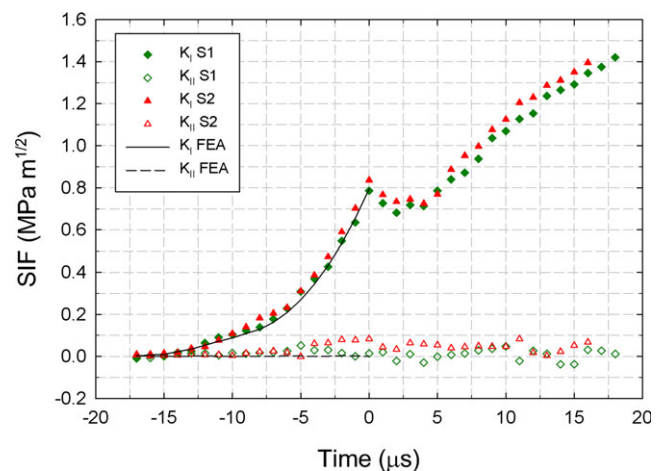


FIGURE 12 Stress intensity factors (SIFs) evaluated from experiments for two soda-lime glass specimens S1 and S2 and finite element simulations up to crack initiation ($t = 0$ μ s in these correspond to the crack initiation at original notch tip)

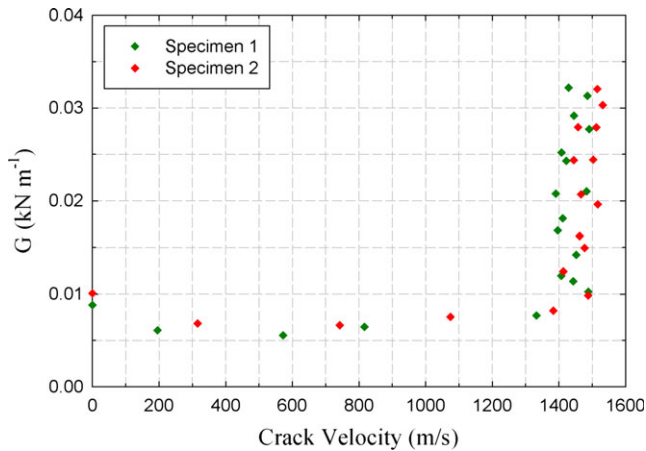


FIGURE 13 Plot of mode-I dynamic strain energy release rates (G) with crack velocity (V) for two soda-lime glass specimens

$$G = \frac{1}{E} [A_I K_I^2 + A_{II} K_{II}^2] \quad (6)$$

where $A_I = \frac{V^2 \alpha_L}{(1-\nu) C_s^2 D}$, $A_{II} = \frac{V^2 \alpha_S}{(1-\nu) C_s^2 D}$, and $D = 4\alpha_L \alpha_S - (1 + \alpha_S^2)^2$. Other parameters have been defined previously (note that the contribution of the second term on the right-hand side of Equation (6) is negligible during dominant mode-I crack growth). After a marginal reduction after crack initiation ($V = 0$), the G values are nearly constant until about 1300 m/s as seen in Figure 13. Beyond this, a rapid increase in the crack driving force over a rather narrow velocity range of 1300-1500 m/s can be seen.

5 | CONCLUSIONS


The transmission-mode DGS method has been extended in this work to visualize and quantify orthogonal stress gradient fields in soda-lime glass under stress wave loading conditions. Typical challenges of studying failure of high stiffness and low toughness transparent ceramics have been overcome in this methodology. Furthermore, the feasibility of DGS to map stress gradient for stress wave loading conditions using ultrahigh-speed digital photography at 1 million frames per second has been demonstrated for two different problems. First, stress gradient fields due to a transiently applied line-load from a Hopkinson bar on the edge of a free-standing glass plate were mapped. The optical fields have been analyzed over-deterministically using least-squares method to evaluate applied force history which was found to match well with that measured from the strain gage instrumentation on the Hopkinson bar. Next, crack-tip fields generated during reverse impact on an edge cracked plate was studied. The evolution of instantaneous optical fields around the crack-tip has been visualized before crack initiation and during fast fracture. The

challenges associated with locating the crack-tip when a hairline crack grows in glass at speeds of ~ 1500 m/s have been addressed and stress intensity factor histories have been successfully extracted. The critical value of SIF at crack initiation was measured as $0.81 \text{ MPa}\sqrt{\text{m}}$. The two orthogonal stress gradient fields have been used in conjunction with a higher-order least-squares based integration scheme to obtain $(\sigma_x + \sigma_y)$ maps around rapidly moving crack-tip. The dynamic crack growth resistance behavior of soda-lime glass has been quantified by evaluating the energy release rate as a function of crack velocity. The resulting ‘elbow’ shaped characteristic reveals a rapid increase in crack growth resistance from approx. 10 to 30 J/m^2 once the crack speed reaches 1500 m/s.

ACKNOWLEDGMENTS

The support of the U.S. Army Research Office for this research through grants W911NF-16-1-0093 and W911NF-15-1-0357 (DURIP) are gratefully acknowledged.

ORCID

Balamurugan M. Sundaram  <http://orcid.org/0000-0002-7355-8369>

Hareesh V. Tippur  <http://orcid.org/0000-0002-5773-8853>

REFERENCES

- Patel PJ, Gilde GA, Dehmer PG, McCauley JW. Transparent armour. *AMPTIAC Newsletter*, Fall. 2000;4:1-16.
- Bourne NK, Rosenberg Z, Mebar Y, Obara T, Field JE. A high-speed photographic study of fracture wave propagation in glass. *Journal De Physique IV Colloque*. 1994;04:C8635-C8640.
- Doll W. Investigation of the crack branching energy. *Int J Fract*. 1975;11:184-186.
- Park H, Chen W. Experimental investigation on dynamic crack propagating perpendicular through interface in glass. *J Appl Mech*. 2011;78:051013.
- McCauley JW, Strassburger E, Patel P, Paliwal B, Ramesh KT. Experimental observations on dynamic response of selected transparent armor materials. *Exp Mech*. 2013;53:3-29.
- Gross SP, Fineberg J, Marder M, McCormick WD, Swinney HL. Acoustic emissions from rapidly moving cracks. *Phys Rev Lett*. 1993;71:3162-3165.
- Takahashi K, Arantani SI, Yamauchi YJ. Dynamic fracture in zone-tempered glasses observed by high-speed photoelastic colour photography. *J Mater Sci Lett*. 1992;11:15-17.
- Aratani S, Ojima H, Takayama K. Holographic interferometric observation of float glass plate fracture by shock tube method. *Proc SPIE*. 2001;4183:1025.
- Aratani S, Yamauchi Y, Kusumoto J, Takahashi K. Dynamic fracture process of thermally tempered glass studied by the method of caustics. *J Ceram Soc Jpn*. 1993;101:804-808.

10. Periasamy C, Tippur HV. Measurement of orthogonal stress gradients due to impact load on a transparent sheet using digital gradient sensing method. *Exp Mech.* 2013;53:97-111.
11. Sundaram BM, Tippur HV. Dynamic crack growth normal to an interface in bi-layered materials: an experimental study using digital gradient sensing technique. *Exp Mech.* 2016;56:37-57.
12. Sundaram BM, Tippur HV. Dynamics of crack penetration vs. branching at a weak interface: an experimental study. *J Mech Phys Solids.* 2016;96:312-332.
13. Sundaram BM, Tippur HV. Dynamic mixed-mode fracture behaviours of PMMA and polycarbonate. *Eng Fract Mech.* 2017;176:186-212.
14. Sundaram BM, Tippur HV. Full-field measurement of contact-point and crack-tip deformations in soda-lime glass. Part-I: quasi-static loading. *Int J Appl Glass Sci.* 2017;00:1-9. <https://doi.org/10.1111/ijag.12278>.
15. Pan B, Qian K, Xie H, Asundi A. Two-dimensional digital image correlation for in-palme displacement and strain measurement: a review. *Meas Sci Technol.* 2009;20:062001(17 pp).
16. Kirugulige MS, Tippur HV, Denny TS. Measurements of transient deformations using digital image correlation method and high-speed photography: application to dynamic fracture. *Appl Opt.* 2007;46:5083-5096.
17. Jajam KC, Tippur HV. Quasi-static and dynamic fracture behaviour of particulate polymer composites: a study of nano- vs. micro-size filler and loading-rate effects. *Compos B.* 2012;43:3467-3481.
18. Lee D, Tippur HV, Phillip B. Quasi-static and dynamic fracture of graphite/epoxy composites: an optical study of loading-rate effects. *Compos B.* 2010;41:462-474.
19. Yoneyama S, Ogawa T, Kobayashi Y. Evaluating mixed-mode stress intensity factors from full-feild displacement fields oobtained by optical methods. *Eng Fract Mech.* 2007;74:1399-1412.
20. Jin H, Bruck HA. Pointwise digital image correlation using genetic algorithms. *Exp Tech.* 2005;29:36-39.
21. Poissant J, Barthelat F. A novel "subset splitting" procedure for digital image correlation on discontinous displacement fields. *Exp Mech.* 2010;50:353-364.
22. Miao C, Sundaram BM, Huang L, Tippur HV. Surface profile and stress field evaluation using digital gradient sensing method. *Meas Sci Technol.* 2016;27:095203(16 pp).
23. Jain AS, Tippur HV. Extension of reflection-mode digital gradient sensing method for vizualizing and quantifying transient deformations and damage in solids. *Opt Lasers Eng.* 2016;77:162-174.
24. Andrews EH. Stress waves and fracture surfaces. *J Appl Phys.* 1959;30:740-743.
25. Gong J, Chen Y, Li C. Statistical analysis of fracture toughness of soda-lime glass determined by indentation. *J Non-Cryst Solids.* 2011;279:219-223.
26. Geandier G, Denis S, Mocellin A. Float glass fracture toughness determination by Hertzian contact: experiments and analysis. *J Non-Cryst Solids.* 2003;318:284-295.
27. Nyongue A, Bouzid S, Dossou E, Azari Z. Fracture characterization of float glass under static and dynamic loading. *J Asian Ceramic Soc.* 2016;4:371-380.
28. Ravi-Chandar K. *Dynamic Fracture.* San Diego: Elsevier; 2004.

How to cite this article: Sundaram BM, Tippur HV. Full-field measurement of contact-point and crack-tip deformations in soda-lime glass. Part-II: Stress wave loading. *Int J Appl Glass Sci.* 2018;9:123-136. <https://doi.org/10.1111/ijag.12289>